Available online at www.sciencedirect.com
SCIENCE DIRECT
Journal of Molecular Catalysis A: Chemical 235 (2005) 302–310
JOURNAL OF MOLECULAR CATALYSIS A: CHEMICAL
www.elsevier.com/locate/molcata

Effects of preparation methods on properties of $Ni/CeO_2–Al_2O_3$ catalysts for methane reforming with carbon dioxide

Jixiang Chen [a,*], Rijie Wang [a], Jiyan Zhang [a], Fei He [b], Sen Han [b]

[a] *Department of Catalysis Science and Engineering, School of Chemical Engineering and Technology, Tianjin University, Tianjin 3000072, PR China*
[b] *Key Laboratory of Green Chemical Technology, Tianjin University, Tianjin 300072, PR China*

Received 23 October 2004; received in revised form 5 April 2005; accepted 6 April 2005
Available online 13 May 2005

Abstract

Xerogel and aerogel catalysts have been prepared via a sol–gel process followed by conventional drying and supercritical drying, respectively. The catalysts were characterized by means of XRD, XPS, H_2-TPR, TPD, TEM, TGA and N_2 adsorption–desorption. The catalytic performance of the catalysts in CH_4 reforming with CO_2 was evaluated. The results indicate that the method for the preparation of the aerogel leads to higher specific surface area, larger pore size, lower bulk density, higher thermal stability, and higher dispersivity and homogeneity of nickel species than that of the xerogel. The aerogel catalyst shows high catalytic activity, good resistance to sintering at high reaction temperature and prolonged stability.

Keywords: Catalyst; CH_4 reforming with CO_2; Aerogel; Xerogel; Supercritical drying

1. Introduction

In recent years, methane reforming with carbon dioxide has drawn enormous attention. This novel process directly converts two low-value greenhouse gases to the synthesis gas with low H_2/CO ratios [1–5], which is a valuable feed for important processes, such as Fischer–Tropsch synthesis and carbonyl synthesis.

The research on the catalysts for this reaction has been mainly focusing on the following issues: (1) the relationship between the intrinsic property and the activity of various metal species; (2) the improvement of resistance towards coke formation; (3) the development of suitable support to enhance the efficiency of the catalyst and (4) the reaction mechanism. Among the supported metal catalysts for methane reforming, the nickel and the noble metal based catalysts showed quite promising catalytic activity [6]. As noble metals are expensive and of limited availability, nickel-based catalysts are preferred for industrial practice [7,8]. Alumina is most often used as a support for reforming catalysts, owing to its high thermal stability and the ability to form spinel structure with many metal oxides. It is very important to immobilize metal species on catalyst surface, which remarkably hinders the sintering of metal crystallites especially at a high reaction temperature [9]. In many literatures, alkali and alkaline-earth metal oxides as well as rare earth oxides are usually added to the nickel-based catalysts for methane reforming, as promoters to optimize the activity of the catalysts [10–13]; ceria is one of the best promoters among all rare earth oxides. Ceria possesses a high oxygen storage capacity and can absorb and release oxygen reversibly in responding to the oxygen concentration in the gas-phase [14]. Its presence shows beneficial effect on the catalyst performance, such as improving the dispersion of the active species, delaying the transition of alumina support from γ-Al_2O_3 to low-surface-area phase α-Al_2O_3 [15,16]. It has been demonstrated by several research groups that the addition of ceria as a promoter can

* Corresponding author. Tel.: +86 22 27890865; fax: +86 22 27890865.
E-mail address: jxchen@tju.edu.cn (J. Chen).

1381-1169/$ – see front matter © 2005 Elsevier B.V. All rights reserved.
doi:10.1016/j.molcata.2005.04.023

enhance the activity, stability and resistance of coke formation on Ni/Al_2O_3 catalysts in methane reforming with CO_2 [17,18].

It is a common knowledge that, in most of the cases, the physicochemical properties of catalysts varies with the preparation methods adapted, in which the preparation procedure usually plays a key role. Although some researchers have examined the properties of nickel-based catalysts prepared via different methods, studies on the impact of synthetic route to aerogels used as methane reforming catalysts are scantly seen. Aerogels show promising potential in catalytic application due to their unique morphological and physicochemical properties [19]. It has been found that the catalytic performance of aerogels is superior to that of the catalysts prepared by conventional methods such as impregnation, etc. [20,21]. However, to our knowledge by far, there is no detailed comparative study regarding the influence of synthetic procedure on the physicochemical properties of aerogel and xerogel catalysts and their catalytic performance in methane reforming.

In the present work, two series of nickel-based catalysts $NiO–CeO_2–Al_2O_3$, an aerogel and a xerogel, respectively, have been prepared by the sol–gel method but using different drying procedures during preparation. The physicochemical property and the catalytic activity of the catalysts have been evaluated by means of XRD, XPS, H_2-TPR, TPD, TEM, TGA, N_2 adsorption–desorption and CH_4 reforming with CO_2.

2. Experimental

2.1. Catalyst preparation

The nickel-based xerogel and the aerogel catalysts were prepared via the sol–gel method. The typical preparation was as follows: (1) an $Al(OH)_3$ sol was first prepared by adding aqueous ammonia dropwise into an $Al(NO_3)_3$ solution under vigorous stirring. (2) To the above sol, a cerium nitrate solution and a nickel nitrate solution were added successively, then the pH value of the mixture was adjusted to 9 with aqueous ammonia under stirring, and the mixture was aged for additional 1 h to obtain a homogenous gel. (3) After aging, the gel was filtered, washed with distilled water, and finally, divided into two parts for further treatment: one part was dried in an oven at 383 K to obtain a conventional xerogel, while the other part was washed with ethanol, and later loaded with ethanol into an autoclave in order to dry under supercritical conditions (8.0 MPa, 533 K). In the latter case, an aerogel powder was obtained after the treatment for 30 min. (4) The as-made solids were calcined in air at 823 K or 1073 K for 4 h, and the final catalysts were labeled as aNCA series (derived from the aerogel) and as xNCA series (derived from the xerogel), of which the number suffixed to the label was the calcination temperature in the Kelvin scale. For all catalysts, the contents of nickel and ceria were set to 9 wt.% and 3 wt.%, respectively.

2.2. Catalyst characterization

X-ray diffraction (XRD) patterns were obtained with a Rigaku D/MAX-2038 X-ray diffractometer with Cu Kα radiation ($\lambda = 0.15418$ nm). Average crystallite size was estimated from XRD line-broadening by employing Scherrer formula. X-ray photoelectron spectroscopy (XPS) was performed on a PHI1600 ESCA Instrument (XPS) with Mg Kα radiation (1253 eV). The BET surface areas of catalysts were measured by a Quantachrom CHEM-BET 3000 system using static adsorption procedures. The apparent density of the catalyst was measured with a measuring cylinder.

Temperature programmed reduction (TPR) was carried out in a tubular quartz reactor, where 100 mg catalyst was loaded in the thermostatic zone. The reduction was conducted in a flow of $H_2–N_2$ mixture (volume ratio, 8:92) at a heating rate of 10 K/min. The consumption of hydrogen was detected using a thermal conduction detector (TCD).

H_2 temperature programmed desorption (H_2-TPD) was carried out in the same system as described for TPR. After reduction at 1073 K, the sample was cooled down to room temperature in a hydrogen flow and allowed adsorption of hydrogen for 30 min. Then, the flow was switched from hydrogen to nitrogen, and the temperature was elevated at a rate of 20 K/min. The desorbed hydrogen was detected using a TCD.

NH_3 temperature programmed desorption (NH_3-TPD) was also carried out in the same system as described for TPR. The catalyst was pretreated in a nitrogen flow at 823 K for 1 h, and then cooled down to 383 K, and ammonia was introduced with nitrogen as a carrier gas at this temperature. After 30 min, the flow was switched to nitrogen, and the temperature was elevated at a rate of 20 K/min. The desorbed ammonia was detected by a TCD.

The morphology of the catalysts after H_2 reduction and reforming reaction was studied by transmission electron microscopy (TEM, JEOL JEM100-CX-II). The amount of coke deposited on the catalyst was measured by using a Shimadzu TGA-50 instrument.

2.3. Catalytic reaction

Methane reforming with CO_2 was carried out over various catalysts in a fixed bed quartz tube reactor of 8 mm i.d. at atmospheric pressure. All catalysts were reduced in situ in a flow of H_2/N_2 mixture (volume ratio, 10:90) at 1073 K for 30 min prior to the reforming. After the reduction the reactor was cooled down to the set temperature, a feed mixture with a $CH_4/CO_2/N_2$ molar ratio of 5:5:1 was introduced. The gaseous products were analyzed with an online chromatograph equipped with a TCD and a TDX-101 packed column.

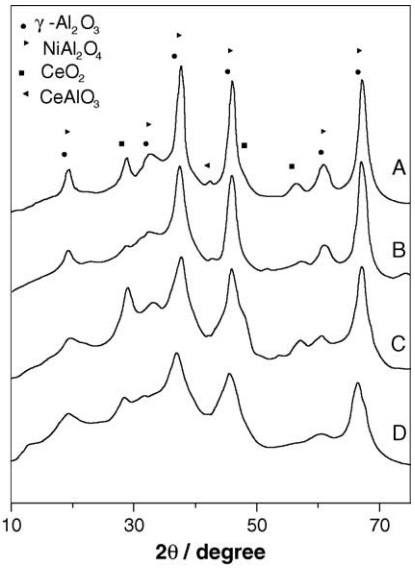

Fig. 1. XRD patterns of aNCA and xNCA series catalysts calcined at 873 K and 1073 K, respectively. (A: xNCA1073; B: aNCA1073; C: xNCA823; D: aNCA823.)

Table 1
XRD analysis data of catalyst samples

Catalyst sample	Peak 3		Peak 5		Peak 8	
	2θ (°)	I/I_1	2θ (°)	I/I_1	2θ (°)	I/I_1
γ-Al_2O_3	37.6	60.0	45.5	65.0	66.4	100
$NiAl_2O_4$	37.0	100	45.0	65.0	65.5	60.0
aNCA823	36.6	76.0	45.2	88.0	65.3	100
xNCA823	37.0	75.0	45.0	86.0	66.2	100
aNCA1073	36.9	78.0	45.1	88.0	66.2	100
xNCA1073	37.1	95.0	45.3	86.0	66.1	100

I/I_1 is the relative intensity of diffraction peaks, dimensionless.

3. Results and discussion

3.1. Physicochemical properties of the catalysts

The phases of the prepared catalysts were characterized by means of XRD. Fig. 1 depicts the XRD patterns of the two series of catalysts. Due to the peak broadening and superimposition of γ-Al_2O_3 and $NiAl_2O_4$ phases, it is difficult to clearly distinguish γ-Al_2O_3 and $NiAl_2O_4$ phases by means of XRD. Therefore, the relative intensity of the main diffraction peaks (listed in Table 1) can be used as a criterion for the presence of phases in catalysts. Three crystalline phases, i.e. γ-Al_2O_3, CeO_2 and $NiAl_2O_4$, were detected in all samples, while $CeAlO_3$ was in addition detected in the samples calcined at high temperature, i.e. aNCA1073 and xNCA1073. The diffraction peaks sharpened as the calcination temperature was raised from 823 K to 1073 K during catalyst preparation, which could be ascribed to the growth of the crystallites. The data listed in Table 1 suggested that nickel species existed mainly in the form of $NiAl_2O_4$, and crystalline nickel oxides were below the detection limit, while cerium species turned to ceria in the catalysts. This is quite reasonable since cerium ions show a higher tendency of hydroxylation than nickel ions. Moreover, the starting pH value for the precipitation of cerium hydroxide is lower than that of nickel hydroxide when the two ions take the same initial molar concentration. During the process of catalyst preparation, nickel species might be isolated by the aluminum hydroxide matrix; thus aggregation of nickel species could be suppressed and the formation of structurally stable spinel phase $NiAl_2O_4$ was favored in a thermodynamic viewpoint. Interestingly, the CeO_2 crystalline phase in the aNCA series was less pronounced than that in the xNCA series. This phenomenon indicated that the dispersion of cerium species was more homogeneous in the aNCA series catalysts than that in the xNCA series. In contrast to the xNCA series catalysts, the relative intensity of the main diffraction peaks over the aNCA samples did not change notably as the calcination temperature was raised from 823 K to 1073 K. This result reveals that the aerogel is more thermally stable than the xerogel. Mizushima and Hori [22] also found that the temperature for γ-alumina transformation into α-alumina in an aerogel was higher than that in a xerogel.

The physical properties of the catalysts are summarized in Table 2. The aNCA series catalysts, i.e. the aerogels, possessed a lower bulk density, a larger pore volume and a higher specific surface area than the xNCA series catalysts, i.e. the xerogels, which obviously resulted from the different methodology employed during preparation. To the common knowledge one may assume that the skeleton of the original sol–gel was almost kept intact in the aerogel, as in the supercritical drying process, and that the influence of surface tension and capillary force on the gel skeleton can be neglected, while in the case of the conventional drying process these may results in a severe impact and even destruction of the original structure of the gel [19].

3.2. TPR results

Fig. 2 shows the TPR profiles of all catalysts. A single, broad reduction peak was observed over all samples, which could be attributed to the reduction of $NiAl_2O_4$ spinel. The

Table 2
Bulk density, specific surface area and pore volume of aNCA and xNCA series catalysts

Catalyst	Calcination temperature (K)	Bulk density (g ml^{-1})	S_{BET} (m^2 g^{-1})	Pore volume (cm^3 g^{-1})
aNCA823	823	0.44	282.9	0.24
xNCA823	823	0.74	195.9	0.18
aNCA1073	1073	0.47	166.0	–
xNCA1073	1073	0.76	111.8	–

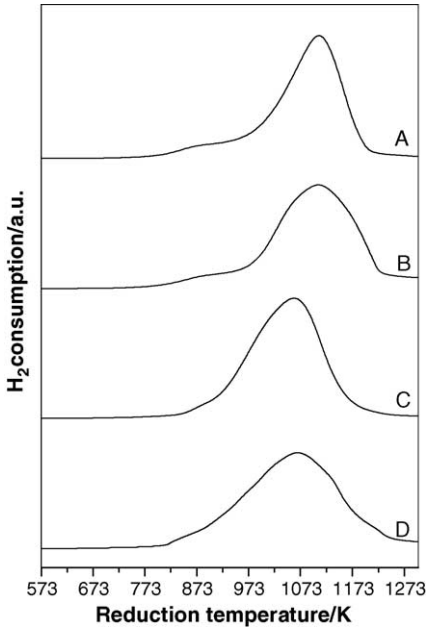

Fig. 2. TPR profiles of xNCA and aNCA series catalysts calcined at 873 K and 1073 K, respectively. (A: aNCA1073; B: xNCA1073; C: aNCA823; D: xNCA823.)

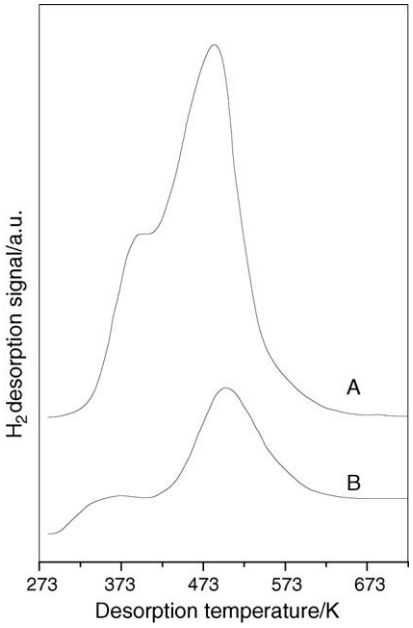

Fig. 3. H_2-TPD profiles of catalysts: (A) aNCA823 and (B) xNCA823.

peaks were centered at around 1063 K in both TPR curves of aNCA823 and xNCA823, and shifted to about 1110 K in those of aNCA1073 and xNCA1073. However, the peaks over the xNCA series catalysts were much broader than those over the aNCA series ones, which suggested again that the nickel species was dispersed more homogeneously in the aerogel catalysts. This meant that, though the sol–gel process could lead to a gel by mixing all species in a sol at an atomic level, the extent of interaction between the nickel species and the support was subject to the post-treatment of the gel. The results also suggested that the aforementioned interaction became stronger with the increase in the calcination temperature. Table 3 shows the quantitative analysis of TPR profiles in Fig. 2. The relative areas of reduction peaks for aNCA1073 and xNCA1073 were smaller than those for aNCA823 and xNCA823, and this meant the reduction degree of the nickel species that existed in aNCA1073 and xNCA1073 were lower. All analysis showed that the result of TPR was consistent with that of XRD.

For ceria to serve as an oxygen storage component, it is essential that the reversible reaction between CeO_2 and Ce_2O_3 takes place easily. According the TPR results of Shyu et al. [23], the CeO_2/Al_2O_3 samples calcinated at 800 °C could be reduced completely below 1000 °C. In Fig. 2, no obvious reduction peaks of CeO_2 existed since they were masked by the reduction peaks of Ni^{2+}.

Table 3
Relative areas of reduction peaks of different catalysts in their TPR profiles

Sample	Relative peak area (a.u.)
aNCA823	4819
xNCA823	4900
aNCA1073	4173
xNCA1073	4096

3.3. H_2-TPD results

H_2-TPD profiles of aNCA823 and xNCA823 are shown in Fig. 3. Two H_2 desorption peaks appeared in all profiles; the peak temperatures over aNCA550 were 391 K and 493 K, while those over xNCA550 were 358 K and 496 K, respectively. Moreover, the areas of the H_2 desorption peaks of aNCA550 were estimated at 2.2 times as large as those of xNCA550. This result suggests that nickel species on aNCA823 were much more homogeneously dispersed than that on xNCA823, which is quite in agreement with the results of XPS and nickel crystallites sizes shown in Table 4. The smaller the nickel crystallites, the larger the specific area of nickel and the desorption amount of H_2 as well.

3.4. NH_3-TPD results

The surface acidity of aNCA823 and xNCA823 were characterized with NH_3-TPD. Fig. 4 depicts the profiles of the catalysts. The adsorption of NH_3 on *a*NCA823 was higher than that on xNCA823; i.e. there were more acid sites on the surface of aNCA823, which could be attributed to the larger specific area of aNCA550.

3.5. XPS results

XPS analysis shed more light on the state of nickel species. The electronic binding energies of $Ni_{2p_{3/2}}$ in aNCA823 and xNCA823 were all 855.9 eV, which were higher than those

Table 4
Crystallite size of nickel on catalysts aNCA823 and xNCA823 before and after reaction

Catalyst sample	Average size of nickel (nm)[a]		Average size of nickel (nm)[b]			
	Before reaction	After reaction	Before reaction	Standard deviation	After reaction	Standard deviation
aNCA823	10.6	12.5	10.8	1.67	12.4	1.6
xNCA823	17.8	21.7	17.7	2.45	20.8	4.1

Note: Catalysts were pre-reduced in H_2 flow at 1073 K for 30 min; reaction conditions were: $CH_4/CO_2/N_2 = 5:5:1$ (molar ratio), $P = 0.1$ MPa, $T = 1073$ K, GHSV = 18 000 ml h^{-1} g^{-1}.

[a] Calculated with Scherrer formula using (2 0 0) reflection of fcc Ni.

[b] Estimated from TEM images.

in pure NiO (855.2 eV). The increase in the binding energy of $Ni_{2p_{3/2}}$ suggested that the interaction between the nickel species and the support was stronger than that in pure NiO. This was most probably due to the formation of $NiAl_2O_4$ spinel considering the XRD and the TPR results. The atomic ratio of Ni/Al on the surface of aNCA823 was estimated to be 0.075, which was close to the bulk atomic ratio of 0.091 and much higher than that of xNCA823 (0.055), indicating a more homogeneous dispersion of nickel species on the surface as well as in the bulk of aNCA823.

3.6. Relationship between catalytic performance and physicochemical properties of the catalysts

The catalysts were tested in the reaction of CH_4–CO_2 reforming. Under the conditions of 18 000 ml g^{-1} h^{-1}, 1073 K and $CH_4/CO_2 = 1$, aNCA823 and xNCA823 showed a similar and high catalytic activity, whose methane conversions were 96.81 mol% and 96.52 mol%, respectively. The activities of aNCA823 and xNCA823 decreased with an increase in space velocity; however, aNCA823 exhibited a better activity than xNCA823 (Fig. 5), which might be due to a higher density of and more homogeneous active sites on the surface of aNCA823.

The catalytic stabilities of the two series catalysts were compared in Fig. 6. xNCA823 and aNCA823 showed almost the same initial activity, and during the first 10 h methane conversions over the two catalysts kept almost steady. However, after 10 h running on stream, the reforming activity of xNCA823 declined sharply while that of aNCA823 remained unchanged within 24 h. The result indicated that aNCA823 had better stability than xNCA823.

In this study, CeO_2 was used as a promoter for its positive effects on the reactivity of Ni/Al_2O_3 catalysts for CH_4 reforming with CO_2. According to Xu et al. [24], CeO_2 as a promoter influenced Ni/Al_2O_3 used for CH_4 reforming with CO_2 in two respects. First, the addition of CeO_2 to Ni/Al_2O_3 could shift the reforming reaction to lower temperature and improve the Ni dispersion; second, there was electronic interaction between CeO_2 and Ni, which was beneficial to inhibiting carbon deposition. Yang et al. [25] provided an explanation for interaction between Ni and CeO_2. It is well known that CeO_2 is a typical n-type semiconductor [26]. In the reforming reaction, H_2 originating from CH_4 decomposition could reduce CeO_2, thus a certain quantity of electron-rich oxygen vacancies being produced. It was easy for the oxygen vacancies to release free electrons and to migrate from the CeO_2 through the Ni–CeO_2 interface to the Ni^0 center, thus increasing the *d*-electron density of the Ni atom. The electron-rich character of the Ni atom naturally inhibited the cracking of CH_4; however, it was favorable for CO_2 to be adsorbed and activated, thus leading to an enhancement of the carbon elimination reaction. In additional, because CeO_2

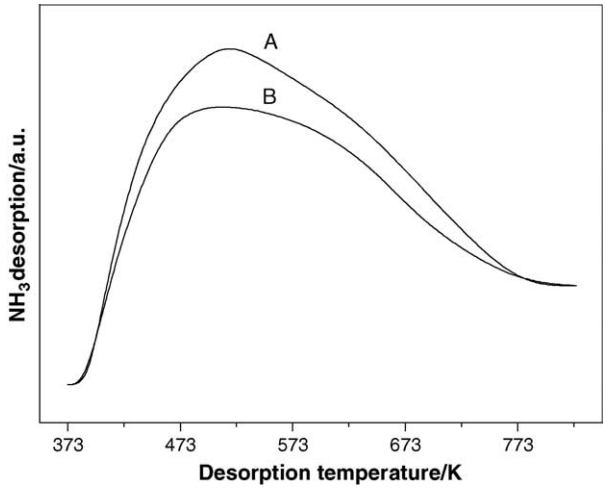

Fig. 4. NH_3-TPD profiles of catalysts: (A) aNCA823 and (B) xNCA823.

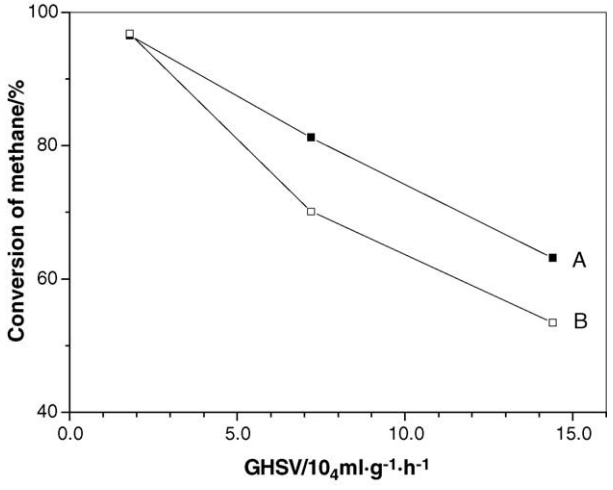

Fig. 5. Effect of space velocity on reforming activity of catalysts: (A) aNCA823 and (B) xNCA823.

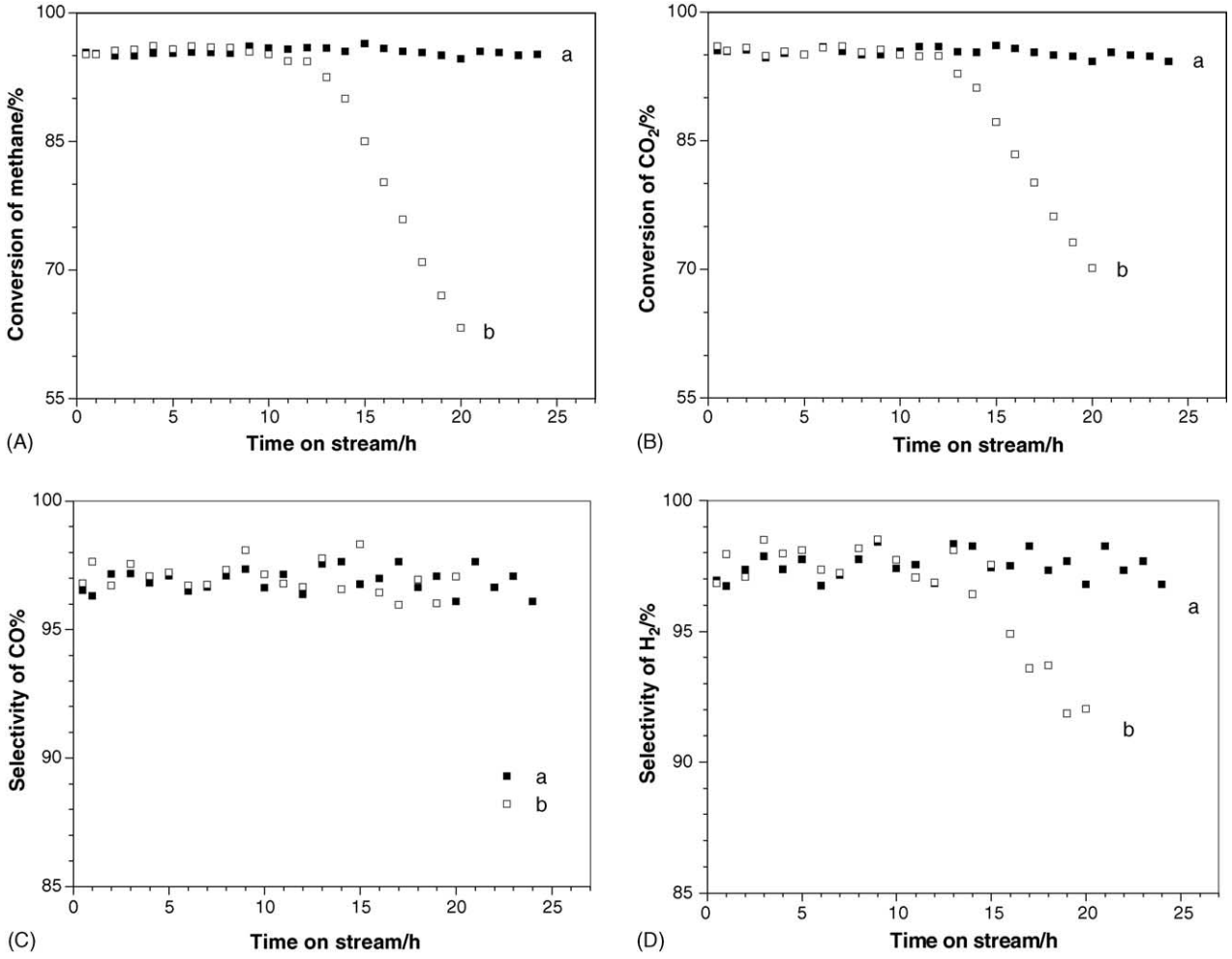

Fig. 6. (A) Methane conversion, (B) CO_2 conversion, (C) CO selectivity and (D) H_2 selectivity as a function of time on stream over pre-reduced catalysts (a) xNCA823 and (b) aNCA823. [Reduction conditions: H_2, 1073 K, 30 min; reaction conditions: $CH_4/CO_2/N_2$ = 5:5:1 (molar ratio), P = 0.1 MPa, T = 1073 K, GHSV = 18 000 ml h^{-1} g^{-1}.]

is basic, it is favorable to adsorb CO_2 and so eliminate the carbon deposition. CeO_2 could be a structural promoter as well. Shyu et al. [23] also suggested CeO_2 could improve the thermal stability of Al_2O_3. The results of XRD showed the dispersion of CeO_2 in aerogel catalysts, i.e. aNCA823 and aNCA1073, was more homogenous than that in xerogel catalysts. Compared with the xerogel catalysts, the homogeneity of CeO_2 in the aerogel catalysts could be more beneficial to the improvement in the thermal stability of Al_2O_3 and the prevention of sintering of nickel crystallites. This was one of the reasons for better reaction stability of aNCA823 compared to xNCA823.

To further elucidate the impact of the preparation method on the properties of the catalysts, more detailed characterization were conducted with the two samples. Fig. 7 presents the XRD patterns of aNCA823 and xNCA823 after reduction and the catalytic test as well. There were mainly two crystalline phases, i.e. γ-Al_2O_3 and Ni^0 in the reduced samples, while graphitic coke was in addition detected on the samples after the catalytic test, which meant that the coke was formed on the catalysts during the reaction. It can be seen from Table 4 and Fig. 8 that the average size of nickel crystallites on aNCA823 was smaller than that on xNCA823 both before and after the reaction. It seems that the extent of nickel crystallites grew during the reforming on aNCA823 was less than that on xNCA823. These results demonstrated that the nickel species on aNCA823 showed better resistance to sintering by taking the advantage of higher dispersivity and homogeneity. The higher dispersivity and homogeneity of nickel species in aNCA823 resulted from its preparation process with supercritical drying and the homogeneity of CeO_2 as above-mentioned.

TGA measurement showed that carbon depositions on aNCA823 after the reaction for 8 h and 24 h were 12.2 wt.% and 14.0 wt.%, respectively, and those on xNCA823 after the reaction for 8 h and 20 h were 5.4 wt.% and 7.3 wt.%, respectively. It was found that more coke was deposited on aNCA823, and the amount of carbon deposition on the catalysts increased with longer time on stream. Coking dynamic process in a TGA study also indicated that coke on the cat-

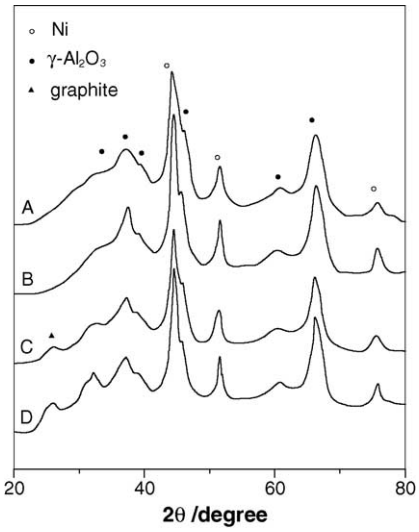

Fig. 7. XRD patterns of catalysts aNCA823 and xNCA823. (A) aNCA823 and (B) xNCA823: after reduction in H_2 at 1073 K for 30 min; (C) aNCA823 and (D) xNCA823: after reaction under the conditions of $CH_4/CO_2/N_2$ = 5:5:1 (molar ratio), P = 0.1 MPa, T = 1073 K, GHSV = 18 000 ml h^{-1} g^{-1}.

alysts generally increased fast in the beginning of reaction (about 5–10 min), and later it increased very slowly [27]. Wang and Lu [28] reported a similar phenomenon.

XPS analysis of C_{1s} (Fig. 9 and Table 5) revealed that there were four kinds of carbonaceous species on the surface of aNCA823 and xNCA823 after reaction. However, the compositions of these species on aNCA823 and xNCA823 were slightly different. Generally, carbonaceous species whose electronic binding energies exist in the ranges of 280.6–282.8 eV, ~284.6 eV and 287.7–290.1 eV can be assigned to carbide, graphite and carbonyl (or carbonate) species, respectively [29,30]. The carbide species were much more pronounced on aNCA823, whereas the graphitic species were on xNCA823.

The primary reasons for deactivation of nickel catalysts can be generally ascribed to coke (or carbon) deposition on the catalysts and the sintering of nickel crystallites. XRD and TEM results demonstrated that the size of nickel crystallites on aNCA823 was smaller than that on xNCA823 after reaction, which rendered aNCA823 higher activity and stability than those of xNCA823.

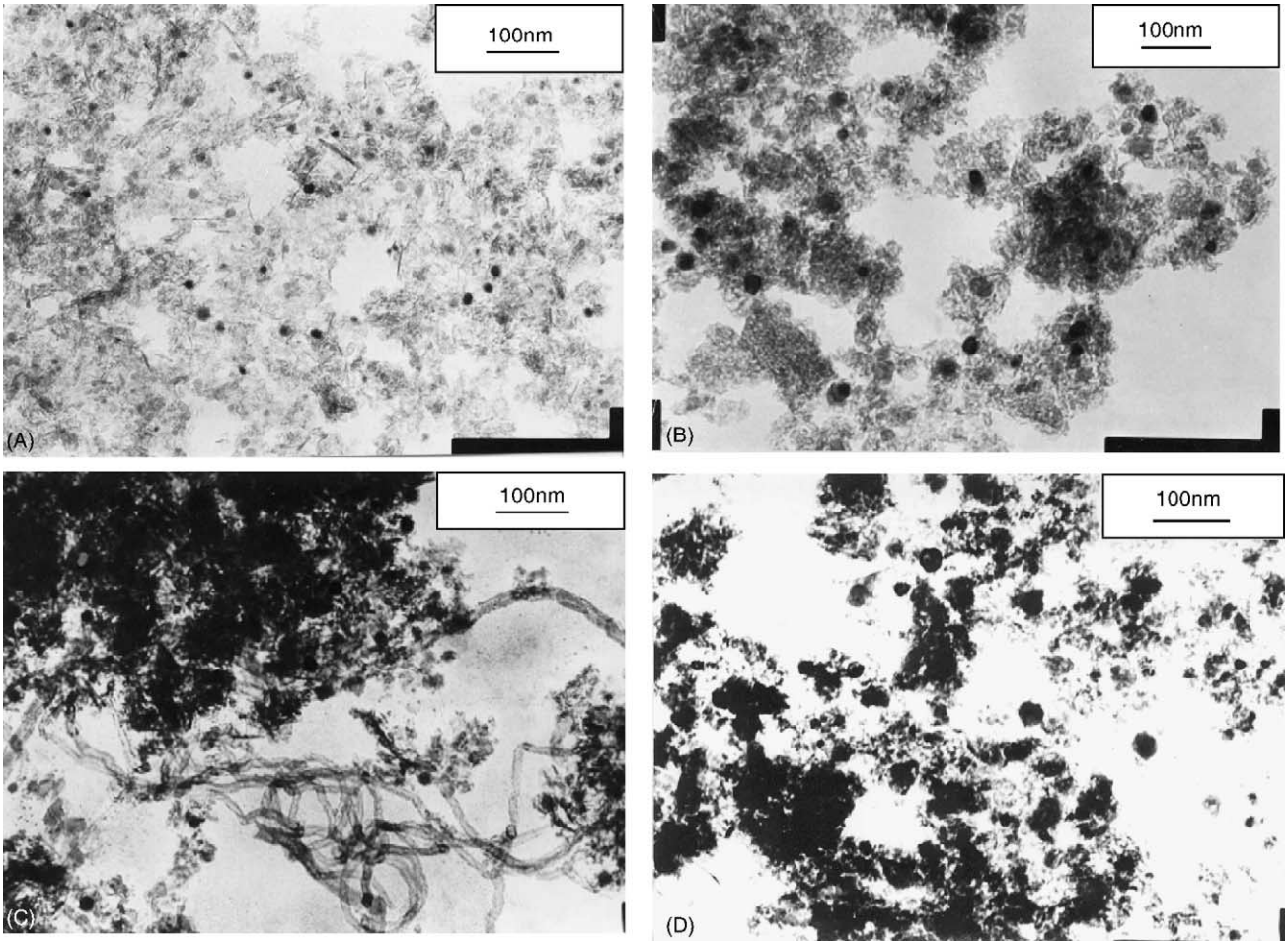

Fig. 8. TEM images of catalysts. (A) aNCA823 and (B) xNCA823: after reduction in H_2 at 1073 K for 30 min; (C) aNCA823 and (D) xNCA823: after reaction under the conditions of $CH_4/CO_2/N_2$ = 5:5:1 (molar ratio), P = 0.1 MPa, T = 1073 K, GHSV = 18 000 ml h^{-1} g^{-1}.

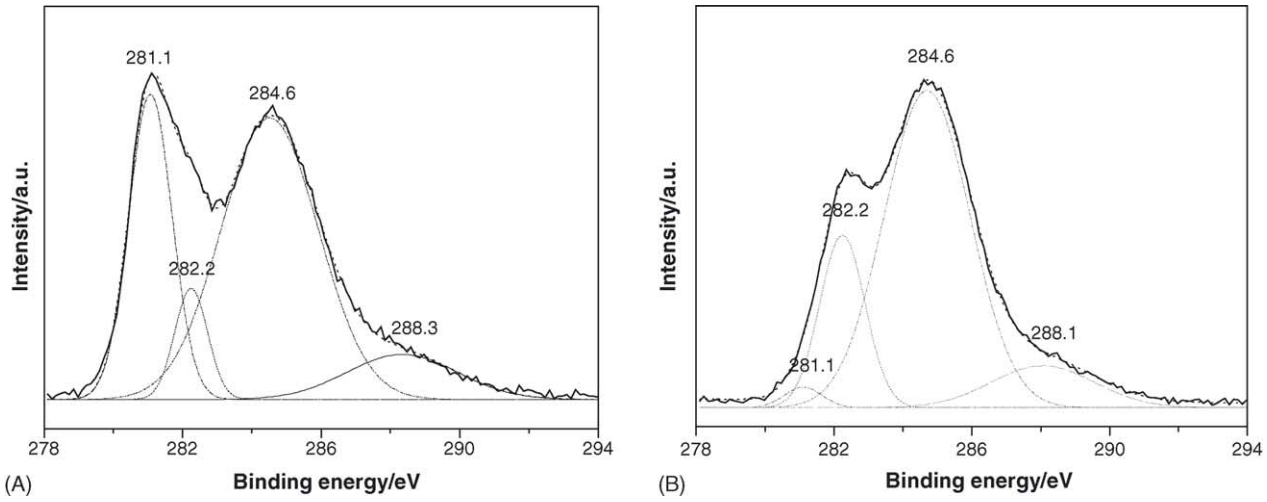

Fig. 9. XPS spectra of C_{1s} on the surface of catalysts (A) aNCA823 and (B) xNCA823 after reaction.

The formation of coke over nickel catalysts under conditions of steam reforming reaction has been well studied in the literatures. Two different types of carbonaceous species, one deactivating (encapsulating carbon) and the other non-deactivating (whisker carbon), were generally found [31]. Chen and Ren [32] reported that filamentous carbon with a hollow inner channel would form on the surface of 10 wt.% Ni/γ-Al_2O_3 catalysts, over which the activity remained during the tests lasted for 120 h. Shi et al. [33] also reported that two types of carbon (amorphous and graphitic) formed on 10 wt.% Ni/γ-Al_2O_3 during methane dehydrogenation. The morphology of graphitic carbon was that of carbon filaments. The amorphous carbon could be eliminated by CO_2, while the graphitic carbon could not due to its longer filament and the distance from the nickel particles. Matsukata et al. [34,35] studied the decomposition of CH_4 and the gasification of deposited carbon with CO_2 over Ni/SiO_2 catalyst, and observed that the carbon with a moss-like morphology could hardly be gasified and caused deactivation of the catalyst. They found that such a type of carbon was dominant on catalyst with higher loading amounts of nickel. In contrast, filamentous carbon with a graphitic structure, which could be gasified with CO_2, became dominant with decreasing nickel loading. In summary, two types of carbonaceous cokes can be formed on catalysts in methane reforming with CO_2 and their reactivity differed. Both graphitic and amorphous carbons show reactivity toward gasification. Wang and Lu [28] proposed that catalyst deactivation caused by carbon deposition depended on the amount, type and location of the carbon formed. When the deposited carbon covered almost the entire surface of the active sites, the catalyst deactivated rapidly. This was often the case for high nickel loading catalyst. The carbon that had better contact with Ni particles exhibited higher reactivity toward gasification thus leading to slow deactivation or better catalyst stability.

The deactivation caused by carbon deposition in our investigation was concerned. TGA measurements showed that the amount of carbon deposited on aNCA823 was almost twice of that on xNCA823. However, aNCA823 exhibited better stability than xNCA823. This is obviously due to the difference of the types of carbons deposited and their reactivity. As XPS results showed, there were more carbide species on the surface of aNCA823 than on xNCA823. It is a common sense that carbide species and carbonyl species (or arbonate) are more reactive than graphite [30], and some part of the former two species may be the active intermediates in this reforming reaction. In addition, a lot of thin filamentous carbon with a hollow inner channel can be found on aNCA823, while less was found on xNCA823 (shown in Fig. 8). From the foregoing results and discussion, it could be deduced that carbon on aNCA823 was probably deposited around and closely contacted nickel parti-

Table 5
Coke deposition and composition of different carbonaceous species on employed catalysts aNCA823 and xNCA823

Catalyst sample	Coke deposition (wt.%)[a]	Composition of different carbonaceous species (%)[b]			
		Species 1	Species 2	Species 3	Species 4
aNCA823	14.0	26.9(281.1)	7.4 (282.2)	55.5 (284.6)	10.1 (288.1)
xNCA823	7.3	1.9(281.1)	19.5 (282.2)	67.8 (284.6)	10.8 (288.3)

[a] Data obtained after reaction, 24 h for aNCA823, 20 h for xNCA823.
[b] Number in parentheses are the binding energy in eV.

cles. Due to the high dispersivity and homogeneity of nickel species on aNCA823, reactive carbonaceous species could be converted readily, and hence deactivation of aNCA823 resulting from blocking the catalytic active sites by deposited carbon was greatly hindered. Meanwhile, owing to its higher specific surface area, larger pore volume, more active carbonaceous species and better resistance to sintering, aNCA823 catalyst possessed a prolonged stability than xNCA823.

4. Conclusion

In summary, the different post-treatments of gel with supercritical drying and conventional drying affect the structure properties of the $Ni/CeO_2–Al_2O_3$ catalysts, the aerogel and the xerogel. As a consequence, the catalysts demonstrate different catalytic performance in methane reforming with carbon dioxide. The method for the preparation of the aerogel catalyst leads to higher specific surface area, larger pore size, lower bulk density, higher thermal stability, higher dispersivity and homogeneity of nickel species than that of the xerogel. Carbon deposition and nickel sintering are thought to be the main factors causing catalyst deactivation. The aerogel catalyst possesses a better catalytic activity and stability than the xerogel owing to its higher density of active sites on the surface, more active carbon species formed during the reaction and well separation of nickel crystallites. Meanwhile, a higher specific surface area and a larger pore size also lead to the prolonged stability of the aerogel catalyst.

Acknowledgment

This work was supported by the Foundation for Young Teacher in Tianjin University.

References

[1] A.T. Ashcroft, A.K. Cheetham, M.L.H. Green, P.D.F. Vernon, Nature 52 (1991) 225.
[2] K. Tomishige, Y.G. Chen, K. Fujimoto, J. Catal. 181 (1999) 91.
[3] J.B. Claridge, A.P.E. York, A.J. Brungs, C. M-Alvarez, J. Sloan, S.C. Tsang, M.L.H. Green, J. Catal. 180 (1998) 85.
[4] J.H. Bitter, K. Seshan, J.A. Lercher, J. Catal. 176 (1998) 93.
[5] M.C.J. Bradford, M.A. Vannice, J. Catal. 173 (1998) 157.
[6] M.C.J. Bradford, M.A. Vannice, Catal. Rev. Sci. Eng. 41 (1999) 1.
[7] K. Tomishige, O. Yamazaki, Y.G. Chen, K. Yokoyama, X.H. Li, K. Fujimoto, Catal. Today 45 (1998) 35.
[8] J.M. Wei, B.Q. Xu, J.L. Li, Z.X. Cheng, Q.M. Zhu, Appl. Catal. A 196 (2000) 167.
[9] Z. Xu, Y.M. Li, L. Chang, J.Y. Zhang, R.Q. Zhou, Z.T. Duan, Appl. Catal. A 210 (2001) 45.
[10] S.B. Wang, G.Q. Lu, J. Chem. Technol. Biotechnol. 75 (2000) 589.
[11] Z.X. Cheng, Q.L. Wu, J.L. Li, Q.M. Zhu, Catal. Today 30 (1996) 147.
[12] Z. Xu, Y.M. Li, J.Y. Zhang, L. Chang, F. He, Chin. J. Catal. 18 (1997) 364.
[13] J.S. Chang, S.E. Park, H. Chon, Appl. Catal. A 145 (1996) 111.
[14] H.C. Yao, Y.F.Y. Yao, J. Catal. 86 (1984) 254.
[15] J. Soria, J.M. Coronado, J.C. Conesa, J. Chem. Soc., Faraday Trans. 92 (1996) 1619.
[16] C. Morterra, V. Bolis, G. Magnacca, J. Chem. Soc., Faraday Trans. 92 (1996) 1991.
[17] Z.X. Cheng, Q.L. Wu, J.L. Li, Q.M. Zhu, Catal. Today 30 (1996) 147.
[18] S.B. Wang, G.Q. Lu, Appl. Catal. B: Environ. 19 (1998) 267.
[19] G.M. Pajonk, Catal. Today 35 (1997) 319.
[20] D.J. Suh, T.-J. Park, J.-H. Kim, K.-L. Kim, J. Non-Cryst. Solids 25 (1998) 168.
[21] Z. Xu, Y.M. Li, J.Y. Zhang, L. Chang, R.Q. Zhou, Z.T. Duan, Appl. Catal. A 213 (2001) 65.
[22] Y. Mizushima, M. Hori, J. Non-Cryst. Solids 167 (1994) 1.
[23] J.Z. Shyu, W.H. Weber, H.S. Gandhi, J. Phys. Chem. 92 (1988) 4964.
[24] G.L. Xu, K.Y. Shi, Y. Gao, H.Y. Xu, Y.D. Wei, J. Mol. Catal. A 147 (1999) 47.
[25] Y.L. Yang, W.Zh. Li, H.Y. Xu, React. Kinet. Catal. Lett. 77 (2002) 155.
[26] A. Trovarelli, Catal. Rev. Sci. Eng. 38 (1996) 439.
[27] J.X. Chen, Ph.D. Thesis, Tianjin University, China, 2001.
[28] S.B. Wang, G.Q. Lu, Appl. Catal. A 169 (1998) 271.
[29] V.R. Choudhary, S. Banerjee, A.M. Rajput, Appl. Catal. A 234 (2002) 259.
[30] W.Y. Li, J. Feng, K.Ch. Xie, Q. Sun, Chin. J. Fuel Chem. Tech. 25 (1997) 460.
[31] C.H. Bartholomev, Catal. Rev. Sci. Eng. 24 (1984) 67.
[32] Y.G. Chen, J. Ren, Catal. Lett. 29 (1994) 39.
[33] K.Y. Shi, H.Y. Xu, Y.M. Fan, Y.C. Shang, G.L. Xu, Chin. J. Mol. Catal. 10 (1996) 41.
[34] M. Matsukata, T. Matsushita, K. Ueyama, Energy Fuels 9 (1995) 822.
[35] M. Matsukata, T. Matsushita, K. Ueyama, Chem. Eng. Sci. 51 (1996) 2769.